

## Anomalous Transport in Random Fracture Networks

Brian Berkowitz and Harvey Scher

*Environmental Sciences, Weizmann Institute of Science, 76100 Rehovot, Israel*

(Received 15 July 1997)

We show that dominant aspects of contaminant (particle) transport in random fracture networks—non-Gaussian propagation—result from subtle features of the steady flow-field distribution through the network. This is an outcome of a new theory, based on a continuous time random walk formalism, structured to retain the key space-time correlations of contaminants as they are advected across each fracture segment. Particle tracking simulations on these networks exhibit the same non-Gaussian profiles, demonstrating quantitative agreement with the theory. [S0031-9007(97)04494-3]

PACS numbers: 91.60.-x, 47.55.Mh, 92.40.-t

The nature of chemical transport in the geological environment of the Earth's subsurface is often observed to be anomalous. A well studied example is the dispersion of a pulse injection of a tracer in the flow field of a water-saturated heterogeneous porous sediment or fractured hard rock [1,2]. The movement of the tracer plume is anomalous if the transport coefficients are either space or time scale dependent. The spatial dependence is readily explained as due to permeability fields with coherent lengths varying over many scales [3]. The purpose of this Letter is to demonstrate persistent time-dependent anomalies (i.e., non-Gaussian propagation) in a model fracture system—a well connected network with elements of randomly varying lengths, apertures, and orientations (cf. Fig. 1)—in which the spatial scale of observation is much greater than any element size.

Flow and contaminant transport in fractured geological formations is of considerable practical importance, in terms of exploitation and preservation of fractured aquifers. Particular emphasis has been placed on evaluating properties of hard rock formations as potential underground repository sites for the storage of radioactive and toxic industrial wastes [4]. While major efforts have been devoted to develop realistic theoretical models of these processes, predictive capabilities related to real fractured media remain severely limited [5]. In part, this is due to the very nature of fracture networks in the subsurface which precludes complete and detailed mapping of fractures, and thus studies must rely on extrapolation of exposed features to generate a statistical characterization of fracture systems [2], which we denote symbolically as  $\Omega(f)$ . The challenge to further development of the theoretical models is the best use of  $\Omega(f)$ .

The important finding of this work is that dominant aspects of the tracer transport—non-Gaussian propagation—depend on subtle features of the random flow-field distribution  $\Phi(\mathbf{v})$ , determined from steady-state flow through a network generated with even a simple  $\Omega(f)$ ;  $\mathbf{v}$  is the velocity in a fracture segment, e.g., as shown in Fig. 1. Our finding is the outcome of a new approach to this transport problem based on the use of a continuous

time random walk (CTRW) formalism [6]. In this initial application there is a strong interplay between the analytic formalism and extensive simulations of steady flow in numerical discrete fracture models such as in Fig. 1. We map the simulation results onto  $\psi(\mathbf{s}, t)$ , the probability per time for a transition between fracture intersections separated by  $\mathbf{s}$  with a difference of arrival times of  $t$ . In this mapping we retain the key space-time correlations of particles as they are advected across each segment and dispersed by the random velocity field of the network. This approach makes tractable the determination of the full evolution of the contaminant density (plume),  $P(\mathbf{s}, t)$ , in large systems, in both two and three dimensions. The  $P(\mathbf{s}, t)$ , in this Letter, is compared with many realizations of particle tracking simulations (PTS) on the same networks used to obtain  $\Phi(\mathbf{v})$ .

The formalism of CTRW is well documented in the literature [6,7]. It should suffice to simply state the formal solution for  $P(\mathbf{s}, t)$  and stress the new developments we have made in the CTRW in order to apply it to a system where the fractures are randomly distributed in length, aperture, and orientation. We have incorporated: (1) a  $\psi(\mathbf{s}, t)$  that can describe transitions between quasicontinuous displacements  $\mathbf{s}$  as well as at continuous  $t$ , and (2) the method of analytic continuation to enable us to derive a very stable form for the numerical evaluation of the inverse Laplace transform (LT) (which is, generally, notoriously difficult) to obtain  $P(\mathbf{s}, t)$ . The method depends on the analytic properties of  $\Lambda(\mathbf{k}, u)$ , the Fourier transform and

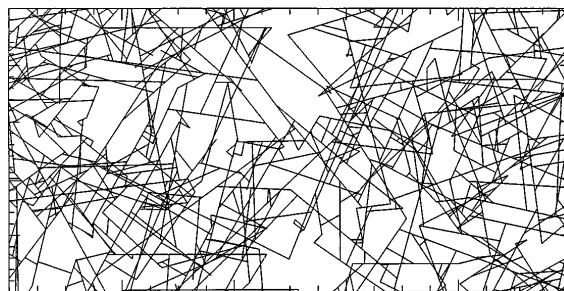


FIG. 1. A 2D fracture network showing only the hydraulically conducting portion or “backbone.”

LT of  $\psi(\mathbf{s}, t)$ , in the complex  $u$  plane (in our case analytic in this plane cut along the negative real axis). Although the  $\psi(\mathbf{s}, t)$ , herein, has been determined explicitly by the flow properties of the random networks, the developments are quite general and can be used for other applications. The solution is

$$P(\mathbf{s}, t) = N^{-d} \sum_{\mathbf{k}} \exp(i\mathbf{k} \cdot \mathbf{s}) \gamma(\mathbf{k}, t), \quad (1)$$

where  $\gamma(0, t) = 1$  and for  $\mathbf{k} \neq 0$

$$\gamma(\mathbf{k}, t) = \int_0^\infty \frac{du e^{-ut}}{2\pi i u} \sum_{\pm} (\pm) \frac{1 - \Lambda(0, u e^{\pm i\pi})}{1 - \Lambda(\mathbf{k}, u e^{\pm i\pi})}, \quad (2)$$

$$\Lambda(\mathbf{k}, u) = \sum_{\mathbf{s}} \exp(-i\mathbf{k} \cdot \mathbf{s}) \int_0^\infty \exp(-ut) \psi(\mathbf{s}, t) dt, \quad (3)$$

and  $\psi(\mathbf{s}, t)$  must be normalized so  $\Lambda(0, 0) = 1$ ;  $N$  is the length of the lattice (spatial domain), and  $d$  is the spatial dimension.

The numerical fracture model employed in this study [8] generates 2D discrete fracture networks and solves for the flow field. In this initial study, the midpoint and orientation of each fracture are uniformly random, and the lengths and apertures are selected from an exponential and lognormal distribution, respectively (cf. Fig. 1). While numerous studies have examined flow and contaminant transport in similar fracture networks, emphasis has been placed on effective hydraulic conductivity and dispersivity [9]; these analyses have not characterized certain key controlling factors which have been clarified in defining a suitable  $\psi(\mathbf{s}, t)$ . After careful examination of a range of correlations, we identified these factors to be the distributions of segment length,

$$p(s) \propto s^{1/2} \exp(-s/s_o), \quad (4)$$

and fluid velocity (leaving fracture intersections) as a function of fracture angle [ $\theta$ , with respect to the pressure gradient (negative), along the  $x$  axis],  $\Phi(\mathbf{v})$ . The coefficient  $s_o$  sets the length scale. In Fig. 2(a) we show a rather unusual ‘‘Viking hat’’  $\Phi(\mathbf{v})$ . Orthogonal to the direction of the pressure gradient,  $\Phi$  is skewed sharply towards small values of  $v$  (the two ‘‘horns’’). More significant is the observation that the distribution falls off exponentially at large  $v$ ,  $\exp[-v/v_0(\theta)]$  with a coefficient  $v_0$  that is strongly  $\theta$  dependent, while the dropoff at small  $v$  is ‘‘soft’’ (algebraic). We can characterize this behavior by

$$\Phi(\mathbf{v}) \propto v^{1+\beta} [\exp(-v/v_0 \cos^2 \frac{\theta}{2}) + w \exp(-v/v' \sin^2 \theta)], \quad (5)$$

where  $\beta$ ,  $w$ ,  $v_0$ , and  $v'$  are parameters of the fit as shown in Fig. 2(b). The second term is needed to fit the horns.

We now put the CTRW and the simulation data together. We can envision all the sites (Fig. 1) with a branch velocity  $\mathbf{v}$ . At each site we can evaluate the fraction  $f(v)$  of the particles entering the branch using a simple mixing rule

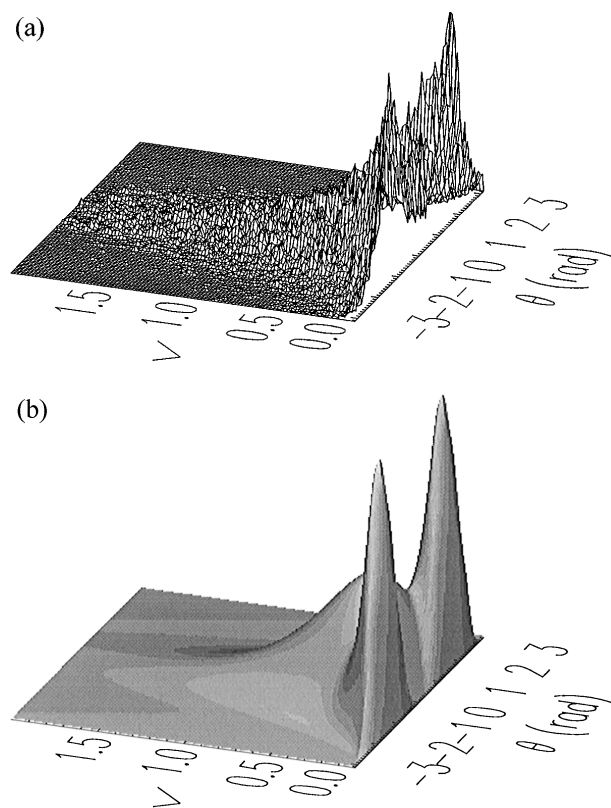


FIG. 2. The fracture-segment velocity distribution  $\Phi(\mathbf{v})$ . (a) A compilation of data from 20 fracture network generations.  $\Phi$  (arbitrary units) vs  $v$  and  $\theta$  (cf. text). The blank space is the intersection with the  $v = 0$  plane. (b) The functional fit with Eq. (5).

[10]. We multiply this term by the probability to encounter the velocity  $\mathbf{v}$  and a displacement  $s$ . Hence

$$\psi(\mathbf{s}, t) = C_n \Phi(\mathbf{v}) p(s) f(v), \quad (6)$$

where  $C_n$  is a normalization constant,  $p(s)$  is given in (4),  $\Phi(\mathbf{v})$  in (5), and the time is determined by  $t = s/v$ . Because of the aperture distribution it can be shown that  $f(v)$  is a slowly varying function of  $v$ , and we will not consider it further in this paper [11]. The long time behavior of  $\psi(\mathbf{s}, t)$  in (6) is determined by the power of  $v$  in  $\Phi(\mathbf{v})$  in (5),  $\psi(\mathbf{s}, t) \rightarrow t^{-1-\beta}$ ,  $t \rightarrow \infty$ . The asymptotic form at large time of  $\psi(\mathbf{s}, t)$  determines [7] the time dependence of the mean position  $\bar{\ell}(t)$  and standard deviation (root mean squared displacement)  $\bar{\sigma}(t)$  of  $P(\mathbf{s}, t)$ .

In the presence of a bias, and for  $0 < \beta < 1$ ,

$$\bar{\ell}(t) \propto t^\beta, \quad \bar{\sigma}(t) \propto t^\beta. \quad (7)$$

The unusual time dependence of  $\bar{\ell}(t)$ ,  $\bar{\sigma}(t)$  is the hallmark of the highly non-Gaussian propagation of  $P(\mathbf{s}, t)$ . This so-called anomalous transport has been very well documented in a large literature of electronic transport measurements in low mobility, disordered semiconductors [12]. The careful determination of  $\beta$ , therefore, is an important and subtle feature of the random velocity distribution that has been overlooked in fracture networks. The probability

to encounter a low velocity on the time scale set by the overall transit time of the plume plays a crucial role in determining the nature of the transport. It is challenging to obtain a very narrow range of  $\beta$  values with our simulation data. However,  $\beta \sim 0.7$  is determined to fit the data well. Equation (7) will be the basis of our quantitative agreement with PTS.

As a first step in the calculation of  $P(\mathbf{s}, t)$ , we evaluate  $\text{LT}\{\psi(\mathbf{s}, t)\}$  of (6). The contribution of the horns (Fig. 2) has been found to be small, so only the first term of (5) for  $\Phi(\mathbf{v})$  is included in (6). There is a simplification [13] if we use  $\beta = 1/2$ ; the contaminant plumes are qualitatively very similar to those using  $\beta \sim 0.7$ , and the main difference is in  $\bar{\ell}(t)$ ,  $\bar{\sigma}(t)$  which we account for using (7). We obtain

$$\Lambda(\boldsymbol{\kappa}, u) = \frac{2}{15\sqrt{\pi}} \int_0^\infty ds s \int_{-\pi}^\pi d\theta e^{-i\boldsymbol{\kappa} \cdot \mathbf{s}^{1/2}} e^{-s} \cos \frac{\theta}{2} \times s \exp(-\sqrt{8su}/\cos \frac{\theta}{2}), \quad (8)$$

where nondimensional variables  $s_0 u / 2v_0 \rightarrow u$ , and  $\boldsymbol{\kappa} \equiv \mathbf{k} s_0$ ,  $s/s_0 \rightarrow s$  are introduced. We replace the lattice sum in (3) by an integral which is exact in the limit  $N \rightarrow \infty$ , and  $\Lambda(0, 0) = 1$ . An analytic expression for  $\Lambda(0, u)$  (details will be given elsewhere) is

$$\Lambda(0, u) = p_1 e^u K_1(u) + p_2 e^u K_0(u) - \sqrt{2\pi} \frac{16}{5} u^{1/2}, \quad (9)$$

where  $K_i(x)$  is the modified Bessel function [14] of order  $i$ ,  $p_1 \equiv (u - \frac{52}{15}u^2 - \frac{16}{15}u^3)$  and  $p_2 \equiv (7u + 4u^2 + \frac{16}{15}u^3)$ . In the limit  $u \rightarrow 0$ ,

$$\Lambda(0, u) \approx 1 - \sqrt{2\pi} \frac{16}{5} u^{1/2} - 7u(\ln u) + \mathcal{O}(u). \quad (10)$$

The appearance of  $u^{1/2}$  as leading term in the small  $u$  behavior of  $\Lambda(0, u)$  derives from  $\psi(\mathbf{s}, t) \sim t^{-3/2}$  for  $t \rightarrow \infty$ . The logarithmic term derives from the specific value of 2 for the power in the exponent in (5).

We evaluate the  $s$  integral in (10) for  $\boldsymbol{\kappa} \neq 0$ ,

$$\Delta(\boldsymbol{\kappa}, u) = 96 \int_{-\pi}^\pi d\theta \cos \frac{\theta}{2} (1 + i\boldsymbol{\kappa} \cdot \hat{\mathbf{s}})^{-7/2} e^{z^2} i^6 \text{erfc}(z), \quad (11)$$

$$z \equiv \sqrt{2u}/[\cos \frac{\theta}{2} (1 + i\boldsymbol{\kappa} \cdot \hat{\mathbf{s}})^{1/2}],$$

where  $\hat{\mathbf{s}}$  is the unit vector  $(\cos \theta, \sin \theta)$  and  $i^n \text{erfc}(z)$  is the  $n$ th repeated integral of the complementary error function [14]. It can be shown that  $\Delta(\boldsymbol{\kappa}, u)$  has the same analytic properties as  $\Lambda(0, u)$  a branch point at  $u = 0$  and analytic in the  $u$  plane with a branch cut along the negative real  $u$  axis. Using the analytic continuation properties of the  $K$ -Bessel functions [14], we can evaluate  $\gamma(\mathbf{k}, t)$  numerically in (2) and finally, the inverse Fourier transform in (1) is computed with the use of standard fast Fourier transform routines.

Figure 3(a) shows a sequence of the average (in the  $y$  direction)  $P(x, t)$  vs  $x$ . The progression of the normalized

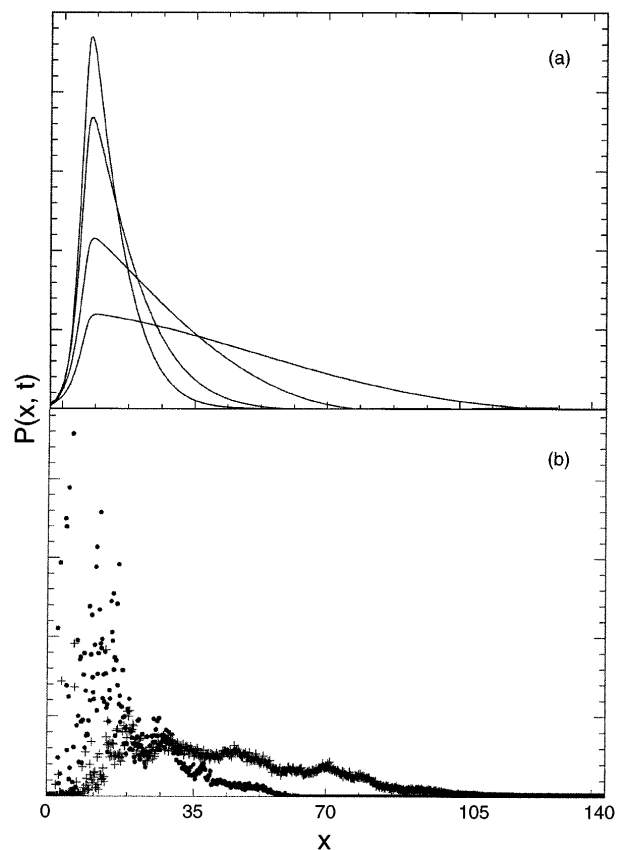


FIG. 3. The average (along the  $y$  axis) of  $P(\mathbf{s}, t)$ , defined as  $P(x, t)$  vs  $x$  (units of length are  $s_0$  and time  $s_0/2v_0$ ). (a) Equation (1) for  $t = 800, 2000, 8000$ , and  $30000$ ,  $\beta = 1/2$ ; (b) Simulation results averaged over 50 realizations for  $t = 20$  ( $\bullet$ ) and  $50$  ( $+$ ),  $\beta \sim 0.8$ . The vertical scale is arbitrary. The large difference in time scales is due to the difference in  $\beta$ .

plume,  $P(x, t)$ , is highly non-Gaussian. The peak of the distribution remains close to the injection point, while a finite fraction of relatively fast particles continually stretches out the concentration profile. The shapes are very similar to the field observations in Fig. 7 of [1]; the  $t$  dependence is also similar (the peak drops by a factor of  $\sim 2.5$  in an order of magnitude of time). The shapes are also similar to propagating packets of electric charge measured directly in amorphous chalcogenides [15].

Contaminant transport by PTS is modeled with a standard routine [8]. Particles move in discrete steps between fracture intersections, plug flow is assumed within each fracture segment, and effects of adsorption, diffusion, and mechanical dispersion within the fractures are ignored. Complete mixing of contaminants is assumed at fracture intersections, and particles leaving an intersection are distributed randomly among outflowing fracture segments in proportion to their volume flow [10]. For each fracture network generation  $\bar{\ell}(t)$ ,  $\bar{\sigma}(t)$ , and  $P(x, t)$  are averaged over a number of initial sites of injection of 5000 particles. In Fig. 3(b) we show two  $P(x, t)$ , at different times, averaged over 50 realizations. Despite some noise,

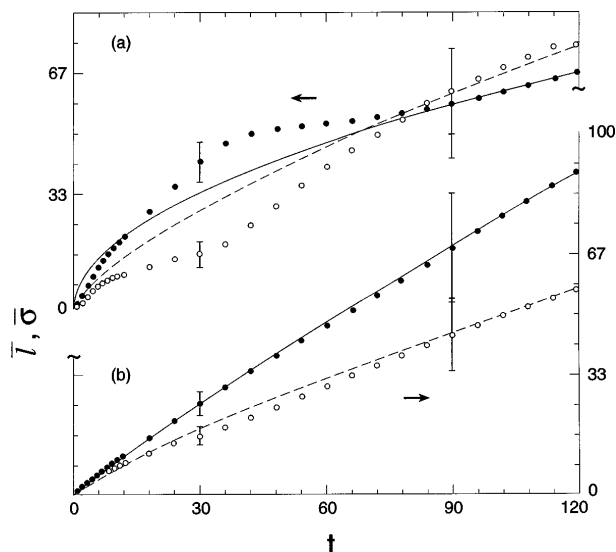


FIG. 4. The mean  $\bar{\ell}(t)$  (●) and standard deviation  $\bar{\sigma}(t)$  (○) of  $P(x, t)$  vs  $t$  (units of length are  $s_o$  and time  $s_o/2v_o$ ). (a) The average over initial sites of one network generation with the fit of (7), with  $\beta \sim 0.5$  (—) and  $\beta \sim 0.7$  (----), respectively. (b) The average of 50 realizations with the fit of (7) with  $\beta \sim 0.9$  (—) and  $\beta \sim 0.8$  (----), respectively. There is an overlap in the error widths of  $\beta$  for  $\bar{\ell}$ ,  $\bar{\sigma}$ .

the plumes clearly exhibit the same qualitative shapes of highly non-Gaussian behavior as the theoretical ones in Fig. 3(a) even though  $\beta > 0.5$ . In Fig. 4(a) we show  $\bar{\ell}(t)$ ,  $\bar{\sigma}(t)$  for one network generation with the best fit to (7) for  $\beta \sim 0.5$  and  $\beta \sim 0.7$ , respectively. Every generation has exhibited the same agreement (with sublinear  $t$  dependence), however, with a different value of  $\beta$  with  $0.5 < \beta < 0.9$ . An average of all these realizations is shown in Fig. 4(b) with  $\beta$  for  $\bar{\ell}(t) \lesssim 0.9$  and for  $\bar{\sigma}(t)$ ,  $\beta \gtrsim 0.8$ . Representative error bars for these averages are shown and the clear deviation of  $\bar{\ell}(t)/\bar{\sigma}(t)$  from the Gaussian dependence of  $\sqrt{t}$  is a signature of anomalous transport. The scant statistics of determining  $\beta$  from  $\Phi(\mathbf{v})$  for each generation does not allow a one-to-one theoretical comparison; however, the value  $\beta \sim 0.7$  obtained for an averaged  $\Phi(\mathbf{v})$ , Fig. 2, is within the error limits of agreement with the  $\beta$  of  $\bar{\sigma}(t)$  in Fig. 4(b). It is remarkable that each generation exhibits anomalous transport.

The PTS data are a satisfactory measure of the behavior of particles, governed by simple flow conditions, traversing a complicated random structure. We have shown in this Letter that this behavior can be accounted for with a theory utilizing a probability density,  $\psi(\mathbf{s}, t)$  (of transitions from each fracture intersection) determined directly from two distributions  $p(s)$ ,  $\Phi(\mathbf{v})$ , characterizing simple aspects

of the geometry and steady-flow properties of the random network. As more complex flow conditions are incorporated into each fracture element of networks generated with a  $\Omega(f)$  derived from field measurements, the anomalous features of the transport will increase. Similar behavior can be expected from highly heterogeneous porous sediments. Therefore we argue that properly modeling the time-scale dependence as well as the spatial scaling is necessary for the explanation of a number of important field observations [1,2]. We are generalizing our approach to deal with this application.

The authors thank Tom Clemo for sharing his computer code and Eli Galanti for assistance. H.S. thanks the Sussman Family Center for partial support.

- [1] J.M. Boggs, S.C. Young, L.M. Beard, L.W. Gelhar, K.R. Rehfeldt, and E.E. Adams, *Water Resour. Res.* **28**, 3281 (1992).
- [2] J.C.S. Long and K. Karasaki, Swedish Nuclear Fuel and Waste Management Co., Stockholm, Technical Report No. 92-06, 1992.
- [3] G. Dagan, *Flow and Transport in Porous Formations* (Springer-Verlag, Berlin, 1989).
- [4] N.A. Chapman and I.A. McKinley, *The Geological Disposal of Nuclear Waste* (John Wiley, Chichester, 1987).
- [5] B. Berkowitz, in *Advances in Porous Media* (Elsevier Science B.V., Amsterdam, 1994), Vol. 2, p. 397.
- [6] H. Scher and M. Lax, *Phys. Rev. B* **7**, 4491 (1973).
- [7] H. Scher and E.W. Montroll, *Phys. Rev. B* **12**, 2455 (1975); M.F. Shlesinger, *J. Stat. Phys.* **10**, 421 (1974).
- [8] T. Clemo, Ph.D. thesis, University of British Columbia, Vancouver, 1994.
- [9] Y.W. Tsang, C.F. Tsang, I. Neretnieks, and L. Moreno, *Water Resour. Res.* **24**, 2049 (1988).
- [10] B. Berkowitz, C. Naumann, and L. Smith, *Water Resour. Res.* **30**, 1765 (1994).
- [11] We estimate that the very low  $v$  part of  $f(v)$  is incorporated into an effective  $\beta$ . An interesting use of the joint  $\psi(\mathbf{s}, t)$  in the framework of Levy flights is in J. Klafter, A. Blumen, and M.F. Shlesinger, *Phys. Rev. A* **35**, 3081 (1987).
- [12] H. Scher, M.F. Shlesinger, and J.T. Bendler, *Phys. Today* **44**, No. 1, 26 (1991).
- [13] G.E. Roberts and H. Kaufman, *Table of Laplace Transforms* (W.B. Saunders Co., Philadelphia and London, 1966).
- [14] *Handbook of Mathematical Functions*, edited by M. Abramowitz and I.A. Stegun (Dover Pub. Inc., New York, 1965).
- [15] S. Imamura, T. Kitamura, and N. Nakamura, *Jpn. J. Appl. Phys.* **23**, L537 (1984).